Calculations of Surface Radiation in Arid Regions—A Case Study

MING-DAH CHOU

Laboratory for Atmospheres, NASA/Goddard Space Flight Center, Greenbelt, Maryland

GUOLIANG JI

Institute of Plateau Atmospheric Physics, Chinese Academy of Sciences, Lanzhou, People's Republic of China

KUO-NAN LIOU, AND SZU-CHENG S. OU

Department of Meteorology/Center for Atmospheric and Remote Sounding Studies, University of Utah, Salt Lake City, Utah

(Manuscript received 13 May 1991, in final form 31 December 1991)

ABSTRACT

The difficulties encountered in the derivation of surface radiation budget in arid regions are studied using the surface and satellite data measured during the preliminary field experiment for the Land–Atmosphere Interactions Experiment conducted at the Heihe River basin in western China. The surface radiation is derived by coupling theoretical radiative transfer calculations with satellite cloud retrievals. Comparisons with the surface measurements of solar and thermal IR fluxes show that a large error in the computed surface fluxes occurs in some cases. The error is attributable to the lack of aerosol data, the uncertainty in cloud retrievals, and the time difference between the surface and satellite measurements.

For cloud-free cases, the modeled downward solar fluxes are systematically larger than the measured fluxes. The major cause of the error appears to be the failure to include aerosols in the calculations. The error is particularly large in the afternoon hours when the ground temperature is very high (>50°C) and the atmosphere dust content is large due to an unstable boundary layer. We find that the error can be reduced and that a good agreement between the computed and measured surface solar fluxes can be obtained by using an aerosol single-scattering albedo of 0.5 and an optical thickness of $\approx$0.2 in the afternoon hours. Nevertheless, the reason for the strong absorption of solar radiation in the atmosphere remains unclear.

For all the cases studied when both surface and satellite data are available, the mean errors are 4.3 and −4.7 W m^{-2} for the net downward surface solar flux and the downward surface IR flux, respectively. The rms errors are 17.4 and 22.1 W m^{-2} for the respective surface fluxes. The relatively large errors found in the cases with small cloud amounts can be explained by the fact that aerosols are often misinterpreted as clouds in the cloud retrievals.

Results of this study reemphasize the importance of aerosols in surface radiation calculations. Because the diurnal variation of ground temperature is very large in the arid regions, reliable calculations of surface IR radiation require high temporal resolution for temperature measurements. Aerosol and ground-temperature retrievals from satellite data should be the highest priority in the computations of surface radiation budget over arid regions.

1. Introduction

The surface radiation is an important component of the global energy budget and is a key to understanding the dynamics of the earth's climate. It has been demonstrated in a number of investigations (e.g., Darnell et al. 1988; Gautier et al. 1984; Gupta 1989; Justus et al. 1986; Pinker and Laszlo 1990; Schmetz 1989) that satellite measurements of reflected and emitted radiation can provide useful information for deriving the large-scale and long-term surface radiation budget. The surface solar radiation can be derived directly from the satellite measurement of radiation at the top of the atmosphere through an empirical relationship. It can also be derived by using a radiative transfer model based on known physics with satellite retrievals of cloud, aerosol, and surface parameters. Because of the uncertainty in the input data used in the radiative transfer calculations, this approach is by no means more accurate than the empirical approach. However, the accuracy of surface radiation calculations can be constantly improved as the quality of the data improves and as we derive a better understanding of physical processes that affect surface radiation.

The degree of difficulty in computing surface radiation varies geographically. In arid and semiarid regions, where the atmospheric dust loading is large, it is difficult to unambiguously infer aerosols and clouds from satellite-measured radiances because both aerosols and clouds have an effect of enhancing reflectivity. Fur-

Corresponding author address: Dr. Ming-Dah Chou, NASA/Goddard Space Flight Center, Laboratory for Atmospheres, Code 913, Greenbelt, MD 20771.

thermore, because the diurnal surface temperature variation is large in arid regions, it requires frequent input of surface temperature to compute the large diurnal variation of surface IR radiation. Since arid and semiarid regions cover a substantial area of the earth, reliable methods for computing the energy budgets in these regions are imperative to global climate studies.

During the period 4–20 September 1988, a preliminary field experiment for the Land–Atmosphere Interactions Experiment was conducted at the Heihe River basin in arid western China. One objective of the experiment was to gain improved understanding of the water and heat budgets in the region and of the role of land–atmosphere interactions on the boundary-layer dynamics. In the preliminary field experiment, the atmospheric temperature and humidity profiles and the surface radiative fluxes were measured. These data, together with the *NOAA-9* Advanced Very High-Resolution Radiometer (AVHRR) radiances, are used in this study to investigate the difficulties encountered in surface radiation calculations. The results of this study can serve as valuable information for further improving radiative transfer models and remote-sensing algorithms. This study can also provide guidance in determining the requirements of future surface and satellite measurements.

2. Surface and satellite measurements

The region of the Land–Atmosphere Interactions Experiment is located in the Heihe River basin (see Fig. 1) with an area of 70×90 km^2 (38°40′–39°40′N, 99°31′–101°00′E). It is in a temperate, arid climate zone. The mean annual precipitation is $\approx$125 mm. The months from April to September account for 85%–90% of the total precipitation. In the spring, persistent wind and desert storms frequently occur. The average

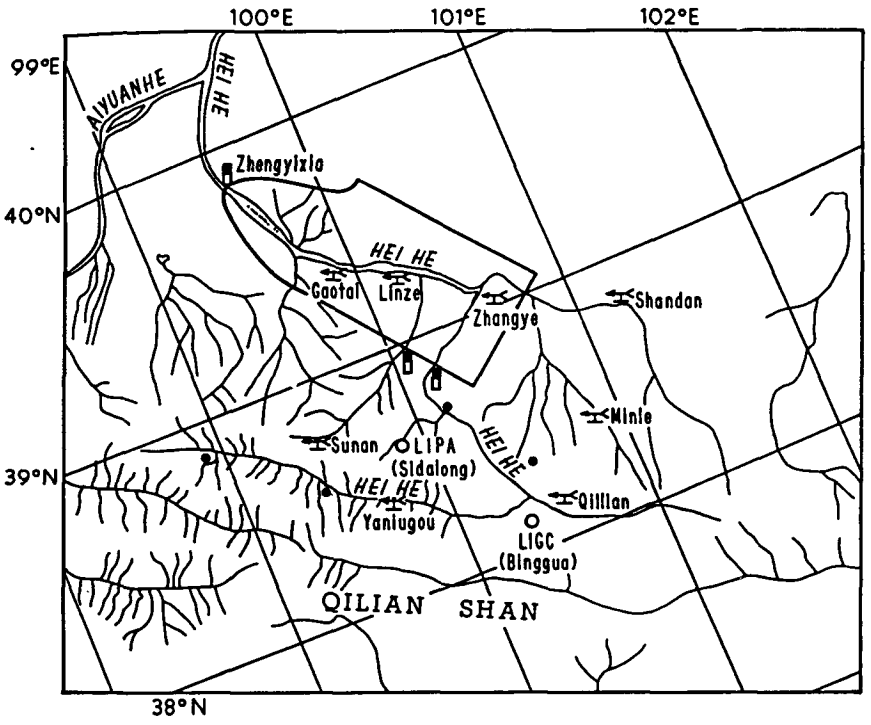

LIGC - The observational station of the Lanzhou Institute of Glaciology and Cryopedology

LIPA - The observational station of the Lanzhou Institute of Plateau Atmospheric Physics

Meteorological station

Hydrographic station

Planned automatic rainfall station

FIG. 1. A general view of the experimental site. The Huayin experimental site is 4–5 km south of Linze.

elevation of the region is about 1.5 km above the sea level. North of the region is the Gobi Desert, which is one of the most important sources for dust particles in the world. South of this area is the Qilian Mountain range (3 km in average elevation above sea level), topped with glaciers. Melting glaciers feed water to the Heihe River, which is an inland river.

The observational network in the basin consists of a number of meteorological stations and experimental sites. The surface radiative fluxes measured at the Huayin experimental site (39°09′N, 100°06′E) are used in this study to validate the surface radiation calculations. The experimental site is flat, consisting of gravels and sand with patchy shrubs. The direct solar flux was measured with an EKO M-52 pyrheliometer. The global (direct + diffuse) downward and the surface-reflected solar fluxes were measured with EKO M-42 pyranometers. The diffuse downward solar flux was also measured with an EKO M-42 pyranometer by introducing a MB-11 light-shading dome to block the direct solar radiation. Adjustments had been made to eliminate the effects of the shade on the diffuse radiation. It has been found that the difference between the global downward solar flux (measured by an EKO pyranometer) and the sum of the direct and diffuse solar fluxes (measured by an EKO pyrheliometer and an EKO pyranometer, respectively) is very small. The upward and downward surface thermal IR fluxes were measured with Epply PIR pyrgeometers. These radiometers were calibrated against an Angstrom pyrheliometer, an EKO pyranometer, and an Epply PIR pyrgeometer, which in turn were calibrated at the National Oceanic and Atmospheric Administration (NOAA) Environmental Research Laboratory (ERL) according to the World Meteorological Organization (WMO) region 4 calibration procedures (TMI, No. 67502). The instruments were mounted 1.5–2 m above the ground. Because the site was selected in a region with rather uniform surface characteristics, the measured fluxes can be considered as representative of a large area surrounding the site.

Calibration of the Angstrom pyrheliometer at ERL for measuring direct solar flux was made with 20 runs that contained 420 sets of data. The calibration constant was determined to be 6.23 with an accuracy of 0.1%. This constant is only 0.3% larger than the original value of 6.21 since its purchase in 1979. Thus, using this instrument to calibrate other direct solar radiometers is reliable. Calibration of the EKO pyranometer at ERL consisted of three parts, which were the determinations of the temperature response, the cosine angular response, and the sensitivity of the radiometer. The temperature response was performed for the range from −35° to 43°C, which is expected to be the temperature range at the Huayin site in September. The temperature response was −0.17% (°C)$^{-1}$ at 25°C and under the condition that the radiative flux is 600 W m^{-2}. In regard to the cosine angular response, observations showed that the standard deviation is 0.0198 for the solar zenith angles from 35.5° to 69.4°. The relative standard deviation was 0.4%, indicating a very good cosine response. To determine the sensitivity of the pyranometer, observations were made for direct and diffuse fluxes. By comparing the fluxes measured by the ERL radiometers, the sensitivity was determined to be 6.9×10^{-3} mV (W m^{-2})$^{-1}$. For a 10-yr period since the pyranometer was placed in use, the sensitivity change was 3%–5%, which is within the range of normal variations of the instrument. For the pyrgeometers, the measured longwave fluxes had been adjusted for the effect of dome temperature according to the guideline given by Epply. Because the pyrgeometers were exposed in the field, the difference between the body and dome temperatures was in the range 1°–2°C, and the flux adjustment can be made accurately.

Thirty-minute mean fluxes were recorded 24 times a day on every hour. In China, there are no time zones. The local standard time of Beijing, which is in the 112.5°–127.5°E time zone, is used throughout the nation. Because Huayin is located at 100°06′E, the local mean solar time (LST) is 1.32 [=(120–100.1)/15] h earlier than the time of the Beijing time zone. For example, 30-min mean fluxes were recorded at 1200 of the Beijing time zone. These fluxes represent the mean values for the period from 1026 to 1056 Huayin local time.

The meteorological station nearest to the Huayin site is located at Zhangye, an oasis about 35 km southeast of the Huayin site. Here radiosonde and surface measurements are available. Upper-air temperature and humidity at 17 standard pressure levels are measured twice a day at 0641 and 1841 LST, while the surface measurements of air temperature and humidity are measured four times a day at 0041, 0641, 1241, and 1841 LST. These data are assumed to be representative of the Huayin site and are interpolated in time for computing surface fluxes at Huayin.

The *NOAA-9* AVHRR Global Area Coverage (GAC) data are used to infer cloud parameters. The *NOAA-9* satellite passes the Huayin area twice a day at ≈0300 LST (descending node) and ≈1600 LST (ascending node). The AVHRR GAC data have a spatial resolution of ≈4 km. There are five channels on the AVHRR; channels 1 and 4 are located, respectively, in the visible spectral region (centered at 0.65 μm) and the infrared (IR) window region (centered at 11 μm), where atmospheric absorption is minimal.

After the satellite was launched, there was no mechanism to directly calibrate the radiances in the solar spectral channels (channels 1 and 2 of the AVHRR). Because the sensors degrade with time, indirect calibration of the radiances is necessary to ensure meaningful interpretation of the satellite data. Holben et al. (1990) and Kaufman and Holben (1992) developed an indirect calibration method based on the reflections over ocean and over desert. They found that the deg-

radation of the channel 1 sensor response from the preflight calibration was 0.77 in 1988. The uncertainty in this degradation factor is 6%. Therefore, in this study, the radiances of channel 1 derived from the preflight calibration are divided by a factor of 0.77 for use in cloud retrievals.

During the experimental observation period 4–20 September 1988, there are only eight cases when both satellite and surface data are available and when the two sets of data are within 1 h of each other. The dates and hours for the satellite and surface measurements are given in Tables 1 and 2, respectively.

3. Radiative transfer calculations

a. Solar radiation

The model of Chou (1992) is used to compute surface solar fluxes. The ultraviolet (UV) and visible region ($\lambda < 0.69$ μm) is grouped into four bands. An effective coefficient for ozone absorption and an effective cross section for Rayleigh scattering were computed for each band. Clouds are assumed to be nonabsorbing in this spectral region. The reflectivity and transmissivity of an atmospheric layer are computed using the delta four-stream discrete-ordinate approximation of Liou et al. (1988). In computing fluxes for a composite of clear and scattering layers, the two-stream adding method (cf., Lacis and Hansen 1974) is used.

In the near-IR region ($\tau > 0.69$ μm), the parameterizations of Chou (1986, 1990) are used to calculate the absorption of solar radiation by water vapor, O_2, and CO_2. The spectrum in this region is divided into seven water vapor absorption bands, and the k-distribution method is applied to individual bands. The cloud single-scattering albedo is specified for the seven absorption bands according to the values given in King et al. (1990). As in the UV and visible region, scattering and absorption of solar radiation by cloud layers are computed using the delta four-stream discrete-ordinate algorithm, and the two-stream adding method is used to compute fluxes for a composite of clear and scattering layers. It is assumed that the ground is Lambertian in both the UV and visible region and the near-IR region.

Desert dusts could have a significant effect on the surface radiation, but there is virtually no information available on the distribution and properties of the dusts in the Huayin region. In order to investigate the sensitivity of surface fluxes to dust particles, it is necessary to specify the dust properties in clear-atmosphere situations.

b. Thermal IR radiation

Calculations of thermal IR fluxes follow the broadband transmission parameterizations given in Chou et al. (1991). These parameterizations are based on line-by-line calculations of transmission functions. The thermal IR spectrum is grouped into two water vapor regions, one CO_2 band (15 μm), one O_3 band (9.6 μm), and a few regions for N_2O and CH_4. The two water vapor regions are noncontiguous; one for band-center regions and the other for band-wing regions. In the water vapor, N_2O, and CH_4 bands, the one-parameter scaling approximation is applied to take into account the effect of pressure and temperature variations along a path. Rather than using the standard conditions for the scaling, the reference pressures and temperatures are chosen to correspond to the heights where cooling is most significant. This choice of the reference pressures and temperatures greatly increases the accuracy of the parameterization. In the CO_2 and O_3 bands, the two-parameter scaling approximation, which is a variant of the Curtis–Godson approximation, is applied to take into account the effect of pressure and temperature variations along a path. The broadband transmission functions are computed using look-up tables in the water vapor and CO_2 bands and are computed from analytical functions, which fit to the line-by-line calculated transmittances, in the O_3, N_2O, and CH_4 bands. Clouds are assumed to be black in the thermal IR region.

TABLE 1. Date, time, solar zenith angle θ_0, satellite zenith angle θ, azimuth angle ϕ, and other parameters for the eight satellite passes. Parameters α_1 and T_4 are the *NOAA-9* AVHRR channel 1 reflectivity and channel 4 brightness temperature (K), respectively. α_c, A_c,τ_c, and p_c are the inferred cloud albedo, amount, optical thickness, and cloud-top pressure (mb), respectively. The cloud parameters are derived using a cloud threshold of 0.35 and a clear-column reflectivity of 0.10.

Date	Local time	θ_0 (°)	θ (°)	ϕ (°)	α_1	T_4 (K)	α_c	A_c	τ_c	p_c (mb)
4 September	1608	64.67	47.73	5.89	0.348	279.0	0.416	0.785	1.4	520
5 September	1557	62.91	36.54	6.38	0.241	302.4	0.350	0.554	2.3	530
6 September	1546	61.18	22.42	7.01	0.202	302.8	0.350	0.382	5.5	530
8 September	1524	57.76	12.25	171.92	0.370	257.7	0.477	0.717	10.4	420
9 September	1513	56.13	27.96	170.96	0.181	295.4	0.532	0.188	9.8	620
10 September	1502	54.58	40.43	170.18	0.149	302.4	0.350	0.198	3.0	620
17 September	1526	61.12	10.36	169.55	0.374	268.9	0.504	0.678	13.5	480
19 September	1505	57.96	39.57	168.31	0.697	232.5	0.697	1.000	11.0	340

TABLE 2. Surface solar and IR flux measurements and calculations. The units are degrees for the solar zenith angle θ_0, fraction for cloud amount A_c, and watts per square meter for the net downward solar flux $S_{net}\downarrow$ and the downward IR flux $F\downarrow$.

Date	Local time	θ_0 (°)	A_c	$S_{net}\downarrow$ (W m^{-2})			$F\downarrow$ (W m^{-2})		
				Measurement	Calculation	Error	Measurement	Calculation	Error
4 September	1641	70.32	0.785	181.8	215.9	34.1	358.3	372.3	14.0
5 September	1541	59.42	0.554	358.8	399.0	40.2	349.0	357.0	8.0
6 September	1541	59.58	0.382	378.0	352.8	−25.3	365.0	341.3	−23.7
8 September	1541	59.70	0.717	231.9	236.0	4.1	375.3	356.5	−18.8
9 September	1441	49.84	0.188	503.0	504.1	1.1	357.1	336.9	−20.2
10 September	1441	50.52	0.198	493.3	527.9	34.6	372.5	334.7	−37.8
17 September	1541	62.89	0.678	212.9	208.1	−4.8	316.6	342.3	25.7
19 September	1441	53.56	1.000	261.2	212.0	−49.2	337.3	352.8	15.5

4. Satellite retrievals of cloud parameters

Surface radiation is sensitive to cloud amount, optical thickness, and height. However, our ability to retrieve these cloud parameters from the satellite-measured radiances is rather limited. In cloud retrievals, an uncertainty of 0.1 in cloud amount, 50% in cloud optical thickness, and 50 mb in cloud height is probably not uncommon. According to Chou (1989), these uncertainties could easily introduce a 50 W m^{-2} error in the surface solar radiation. Although surface radiation is sensitive to clouds, Chou (1989, 1991) has shown that errors induced by the uncertainty in individual cloud parameters largely offset each other if these cloud parameters are inferred by a technique consistent with satellite radiance measurements, that is, if the set of cloud amount, optical thickness, and height inferred from satellite data is in error but can produce the same reflectivity and brightness temperature as measured by the satellite.

When comparing the computed surface fluxes using satellite-inferred cloud parameters with the measured surface fluxes, there are questions concerning the coincidence of these two sets of fluxes in terms of time and space. The time when the satellite passes over the measurement site is not exactly the time when surface fluxes are measured. Because of the uncertainty in navigation, it is difficult to identify the pixels which are exactly over the measurement site. Even if we could identify these pixels that are coincident in time and space with the surface measurements, it is not possible to retrieve the cloud amount, optical thickness, and height from only a pair of radiances measured in the visible- and IR-window channels. Retrieval of cloud parameters often requires additional information concerning the spatial distribution of these radiances. Because of these difficulties, we derive the mean cloud parameters for a 0.25° × 0.25° latitude–longitude region ($\approx$25 × 25 km^2) centered at the Huayin site, instead of estimating the cloud parameters for the site itself. All satellite pixels within this region that are nearest to the time of surface measurements are then used to infer clouds for surface flux calculations.

In this study, the simple threshold method of Chou (1991) is applied to the AVHRR data for estimating the cloud amount, optical thickness, and height. In order to reduce the uncertainty in surface flux calculations induced by errors in cloud retrievals, a specific condition is imposed such that the inferred area-averaged cloud parameters are consistent with the satellite-measured area-averaged radiances. Clouds are usually brighter than the surface, and the presence of clouds is to enhance the reflection of solar radiation. The satellite-measured radiances in the visible channel (channel 1 of AVHRR), where the atmosphere has a minimal effect on the solar radiation, are used to detect the presence of clouds. In the cloud scheme, a threshold α_{th} for the reflectivity in the visible channel is subjectively specified to identify cloudy pixels. If the reflectivity of a pixel is larger than α_{th}, the pixel is identified as "cloudy" (totally cloud filled). It should be noticed that the cloud reflectivity threshold is for identifying cloudy pixels only. Unlike the commonly used cloud–no-cloud threshold method, the threshold α_{th} is not used for identifying clear pixels. The mean cloudy-column reflectivity α_c of a 0.25° × 0.25° latitude–longitude region is computed by averaging the reflectivities of all cloudy pixels. It is assumed that the effect of the atmosphere above clouds on reflectivity is negligible so that the cloud reflectivity is the same as the cloudy-column reflectivity α_c. The mean cloud optical thickness is then estimated from α_c, the solar zenith angle, and the satellite viewing angles using the algorithm developed by Nakajima et al. (1990). Cloud reflectivity is dependent upon the size of cloud droplets. In deriving the cloud optical thickness from α_c, the effective radius of cloud droplets is assumed to be 8 μm.

The mean cloud amount A_c of a 0.25° × 0.25° latitude–longitude region is computed from

$$A_c = (\alpha_1 - \alpha_0)(\alpha_c - \alpha_0)^{-1}, \quad (1)$$

where α_1 is the satellite-measured reflectivity in the visible channel (channel 1 of AVHRR) averaged over the region and α_0 is the clear-column reflectivity. The clear-column reflectivity is estimated from the mini-

mum reflectivities of the Huayin region during the preliminary experiment period. Similar to (1), the cloud amount can also be expressed as

$$A_c = (I_4 - I_0)(I_c - I_0)^{-1}, \quad (2)$$

where I_4, I_0, and I_c are, respectively, the satellite-measured, clear-column, and cloudy-column radiances in the IR-window channel (channel 4 of AVHRR). These quantities are all averaged over a 0.25° × 0.25° latitude–longitude region centered at the Huayin site. With A_c derived from (1), the cloudy-column radiance is then derived from (2) and is given by

$$I_c = [I_4 - (1 - A_c)I_0]\, A_c^{-1}. \quad (3)$$

The clear-column radiance is estimated from the maximum radiances of the Huayin region. As in the visible channel, the effect of the atmosphere above clouds is assumed to be negligible, and the cloud-top temperature is set at the cloudy-column temperature derived from I_c. The cloud-top height is then estimated to be at the level where the atmospheric temperature equals the cloud-top temperature. Since satellite radiance measurements provide virtually no information on the cloud-base height, the cloud-base height is computed by assuming a constant cloud thickness of 50 mb. Errors induced by this assumption are secondary as compared to the uncertainties induced by the cloud amount, cloud optical thickness, and aerosols.

With the use of (1) and (3), the computed cloud amount, optical thickness, and temperature (or height) are consistent with the satellite-measured radiances averaged over a 0.25° × 0.25° latitude–longitude region. It is apparent that the estimated cloud parameters are dependent upon the subjectively specified cloud threshold α_{th}. Nevertheless, it has been shown in Chou (1991) that if α_{th} is reasonably given, the uncertainty in the inferred cloud parameters will not significantly affect the surface radiation calculations.

5. Clear situations

During the preliminary experiment period, the Huayin area is believed to be free of clouds on a few occasions when satellite data are available. Judging from the satellite measurements of radiances and the ground observations of radiative fluxes, the atmosphere is clear at approximately 1518 LST 5, 6, and 10 September 1988. Figure 2 shows the pixels in the reflectivity–brightness-temperature domain within a 0.25° × 0.25° latitude–longitude region centered at Huayin. At these times, the satellite-measured brightness temperature is high in the IR-window channel. It ranges from 297 to 308 K. The radiative temperature for bare land, as deduced from the upward surface IR fluxes measured at Huayin, is approximately 310 K at these times. Thus, the satellite-measured brightness temperature is not much lower than the surface temperature, indicating cloud-free conditions. Furthermore, the reflectivity in-

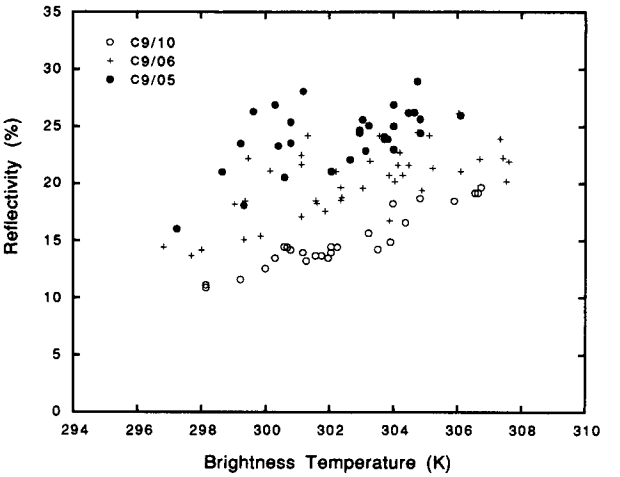

FIG. 2. The reflectivity in channel 1 and the brightness temperature in channel 4 of *NOAA-9* AVHRR for the three clear cases at approximately 1518 LST.

creases with increasing brightness temperature. Because the effect of clouds is to enhance the reflectivity but to reduce the brightness temperature, the reflectivity–brightness-temperature relationship shown in Fig. 2 suggests that the effect of clouds on the satellite measurements is minimal at these times.

The Huayin area is interposed with tributaries of the Heihe River with water derived from melting glaciers. As displayed in Fig. 2, the pixels on the higher-temperature side of the figure reflect bare surface conditions, and those on the other side reflect conditions of partially vegetated surface or water, which have a lower reflectivity and temperature than the bare surface. The satellite-measured reflectivity for the 5 September case is in the 20%–25% range. The brightness temperature for this case is not much different from the 6 and 10 September cases, but the reflectivity is higher by ~5%–10%. This discrepancy could be due to the differences in the satellite viewing angles and the aerosol loading in the atmosphere. The large ranges of the clear-column reflectivity and brightness temperature shown in the figure indicate the difficulty in determining the surface properties from satellite radiance measurements in this arid region.

Of the dates when both satellite and surface measurements are available, 5 September is believed to be the only near cloud-free day. The net downward (downward minus reflected) solar flux measured at Huayin on 5 September is shown in Fig. 3 (solid curve). The surface radiative fluxes normally fluctuate rapidly with time when clouds are present. Thus, the smooth diurnal variation of the surface solar radiation and the large noontime surface flux indicate a rather cloud-free day. Using the temperature and humidity information interpolated from radiosonde and surface measurements and assuming a cloud-free atmosphere and the U.S. Standard Atmosphere ozone profile, fluxes

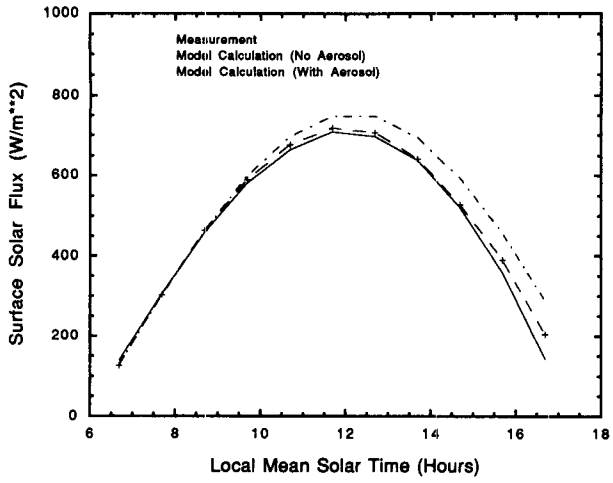

FIG. 3. The diurnal variation of the net downward surface solar fluxes for 5 September 1988. The measured surface flux is shown by the solid curve. The model calculations with and without aerosols are shown by the plus–dash and the dot–dash curves, respectively.

are computed from the radiation routine at 1-h intervals. The broadband surface albedos deduced from the downward and upward fluxes measured at the surface are used in the radiative transfer calculations. The surface pressure is ≈850 mb, and the column-integrated water vapor amount is in the range 0.82–1.44 g cm^{-2} on 5 September 1988. The model-calculated diurnal variation of the net downward solar flux is also shown in Fig. 3 (dot–dash curve). Except in the early morning, the model-calculated net surface solar flux is systematically larger than that of surface measurements. The overestimation increases from approximately 30 W m^{-2} in the late morning to near 145 W m^{-2} in the afternoon.

The computed net downward solar flux is highly asymmetric about noon. It is smaller in the morning than in the afternoon. This asymmetric nature is almost entirely caused by the persistent decrease of surface albedo from morning to afternoon on 5 September 1988. Figure 4 shows the broadband surface albedo measured at the Huayin site on this day. The surface albedo decreases from 0.4 in the early morning to only 0.13 in the late afternoon. Because the measured surface albedo is used in computing surface fluxes, the computed net downward solar flux is smaller in the morning than in the afternoon. It is noted that the measured net downward solar flux is larger in the morning than in the afternoon.

The discrepancy between the model calculations and surface measurements could be attributed to a number of factors: the uncertainties in the radiative transfer model, the atmospheric water vapor and ozone contents, clouds, aerosols, and measurement errors. The parameterization for the absorption of solar radiation by water vapor has been validated against detailed line-by-line calculations (Chou 1986). The discrepancy in the surface radiation between the parameterization and the line-by-line calculations is only ~1 W m^{-2}. Uncertainty in the water vapor and ozone contents might be large, but it cannot explain the large discrepancy between the measurements and model calculations. From model calculations, the surface flux decreases by 2–4 W m^{-2} for an increase of 20% in the water vapor amount and by 1.5–3 W m^{-2} for the same percentage increase in the ozone amount. Clouds could have caused the large discrepancy in the surface solar fluxes, but this situation is not likely as judged from the high brightness temperature shown in Fig. 2. The most likely reason for the large discrepancy is the exclusion of atmospheric aerosols in the model calculations. This view is substantiated by a systematic reflectivity decrease of 10% from 5 to 10 September, as shown in Fig. 2, despite the near-constant brightness-temperature range for the three cases. The persistent decrease of the surface albedo from morning to afternoon as shown in Fig. 4 may also be caused by larger aerosol loading in the afternoon; the surface albedo is smaller for diffuse radiation than for direction radiation when the solar zenith angle is large.

In the arid region, the diurnal variation of surface temperature is large. The measured ground temperature at Zhangye on 5 September increases from 5.9°C at 0641 LST to 57.8°C at 1241 LST. It then decreases to 19.2°C at 1841 LST. The hot surface in the afternoon enhances the static instability and turbulence in the boundary layer, and the atmospheric aerosol content is expected to increase in the afternoon. This is consistent with the smaller net downward surface solar flux measured in the afternoon than in the morning, as shown in Fig. 3. The difficulty in incorporating the aerosol effect in the radiative transfer calculation is that there are no aerosol measurements available and that

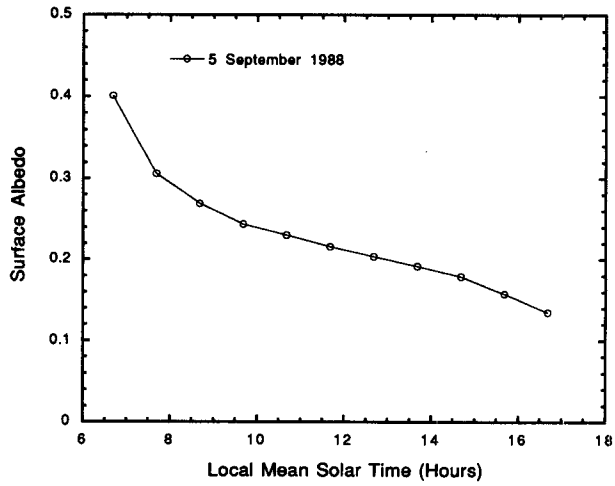

FIG. 4. The broadband surface albedo measured at the Huayin site on 5 September 1988.

the satellite data do not provide adequate information for retrieving aerosol parameters. To address this problem, we must assume a number of different aerosol properties and compare the calculated fluxes with the observed fluxes. Plausible aerosol properties that bring the model-calculated surface fluxes into agreement with the measured fluxes are then indicated.

Aerosol parameters that affect the surface fluxes are the optical thickness, single-scattering albedo, and asymmetry factor. Based on the size distribution of desert aerosols observed in Senegal, Mali, and Niger under various weather conditions, D'Almeida (1987) computed the aerosol single-scattering albedo and asymmetry factor in the spectral region between 0.3 and 4.0 μm. He suggested that the single-scattering albedo be 0.787 in the spectral region 0.3–0.8 μm and 0.851 in the spectral region 0.8–4.5 μm for computing the atmospheric solar fluxes. For the asymmetry factor, the suggested values are 0.774 and 0.853, respectively, for the two spectral regions. We applied these values for the aerosol single-scattering albedo and asymmetry factor, together with the observed humidity profile, to the radiation routine and computed the surface solar fluxes every hour. The net downward surface solar fluxes were made close to the observed values by adjusting the aerosol optical thickness. But when we compared the individual components for surface fluxes, we found that the diffuse downward solar fluxes computed from the model were much larger (>100 W m^{-2} in the late afternoon) than the measurements. The uncertainty in the ozone and water vapor contents affects the solar flux calculations only marginally. On the other hand, the direct and diffuse components of the surface solar radiation are very sensitive to the aerosol single-scattering albedo and asymmetry factor. In order for both the computed direct and diffuse components to be in agreement with the measurements, the aerosol single-scattering albedo and asymmetry factor have to be significantly reduced from the values suggested by D'Almeida (1987).

Using the refractive indices compiled by Shettle and Fenn (1979), Tsay et al. (1991) computed the single-scattering albedo and asymmetry factor for various aerosol mixtures (water, sulfuric acid, dustlike soot, and sea salt) under different humidity conditions. The single-scattering albedo is in the range 0.804–0.904, which is not much different from that deduced by D'Almeida (1987). However, the asymmetry factor is significantly smaller, in the range 0.59–0.73 with a medium value of 0.648. We recomputed the surface solar fluxes by setting the aerosol asymmetry factor at 0.648 and varying the values of optical thickness and single-scattering albedo. A good agreement between the computed and measured surface solar fluxes can be obtained by reducing the aerosol single-scattering albedo to 0.5 and using a time-dependent optical thickness τ computed from

$$\tau(t) = 0.03 + 0.02(t - 7), \quad (4)$$

where t is the local hours (t = 12 at noon). The plus–dash curve in Fig. 3 shows the diurnal variation of the total net downward solar flux at the surface using these aerosol parameters. Figure 5 shows the direct and diffuse components of the measured (solid curves) and computed (dashed curve) downward surface solar fluxes. The agreement between the measured and computed fluxes is good except for the diffuse component during the late-afternoon hours. It should be noted that the aerosol optical thickness and single-scattering albedo are purely empirically chosen to bring the computed fluxes close to the measured fluxes. The diffuse radiation can be made smaller by further reducing the single-scattering albedo, but there is no observational evidence that absorption of solar radiation by desert aerosols is so strong. This heuristic analysis shows the importance of aerosol in affecting the surface solar radiation, but the reason for the very strong absorption of solar radiation in the atmosphere during the late-afternoon hours still remains unclear. One plausible explanation for the small diffuse radiation is the measurement error. The diffuse radiation was measured with an EKO pyranometer by introducing a shade to block the direct radiation. Because the direct radiation is a large quantity, as compared to the diffuse radiation, a small error in the blocking of the direct radiation could introduce a significant error in the diffuse radiation.

The downward IR radiation at the surface is strongly dependent on the near-surface temperature and humidity. Because there are only two radiosonde measurements per day at 0641 and 1841 LST, it is not possible to have meaningful calculations of diurnal surface IR radiation. However, additional information can be derived from the surface measurement of air temperature and humidity at 0641, 1241, and 1841 LST. Instead of computing the diurnal surface IR radiation for 5 September 1988, we compute the IR fluxes at 1541 LST 5 and 6 September and at 1441 LST 10 September near the time of the satellite passes. The upper-air temperature and humidity are taken from the radiosonde measurement at 1841 LST but are adjusted by a factor x_s/x_r, where x_s is the surface air temperature (or humidity) either at 1441 LST or at 1541 LST interpolated from the values measured at 1241 and 1841 LST and x_r is the radiosonde-measured surface temperature (or humidity) at 1841 LST.

The calculated downward IR fluxes at the surface for the 5, 6, and 10 September cases are, respectively, 324.35, 325.60, and 334.72 W m^{-2}. These values are significantly smaller than the measured values, which are 349.0, 365.0, and 372.47 W m^{-2}, respectively, for the three cases. In addition to the uncertainties in the temperature and humidity interpolations, the failure to include aerosols in the calculations might have con-

tributed to the underestimation of the downward IR flux at the surface.

6. General situations

The cloud amount, optical thickness, and height are computed by giving the cloud threshold α_{th} and the clear-column reflectivity α_0. Because there are uncertainties in both α_{th} and α_0, we have chosen various values for these reflectivities to study the sensitivity of surface radiation to these parameters. Analyses of the AVHRR channel 1 reflectivity for the pixels in the immediate neighborhood of the Huayin site show that the minimum reflectivity is in the range of 0.10–0.15, which represents the reflectivity with minimal cloud and aerosol interference (i.e., clear-column reflectivity). The values chosen for the study are 0.10 and 0.15 for α_0 and 0.25 and 0.35 for α_{th}. The inferred cloud reflectivity and amount for $\alpha_0 = 0.1$ and $\alpha_{th} = 0.35$ are given in Table 1 for the eight satellite passes when surface radiation measurements are available. Also given in the table are the optical thickness derived from the cloud reflectivity, the solar zenith angle θ_0, the satellite zenith angle θ, and the azimuth angle ϕ. These cloud parameters are estimated using pixels in the 0.25° × 0.25° latitude–longitude region centered at the Huayin site.

A cloud-free atmosphere with significant aerosol loading is likely to be interpreted as partly cloudy when using satellite data. The reflectivity of many of the pixels for the three "clear" cases (5, 6, and 10 September) shown in Fig. 2 is greater than the expected clear-column reflectivity of 0.1. Although aerosols are probably the most likely factor in enhancing the reflectivity in these cases, clouds could also have the same effect on reflectivity. The Huayin region is interpreted as partly cloudy at those occasions using satellite data. For these clear cases, none of the pixels has a reflectivity greater than the cloud threshold of 0.35, and the cloud reflectivity is set to 0.35. Because the reflectivities for the cases of 5 and 6 September (0.241 and 0.202, respectively) are significantly higher than the assumed clear-column reflectivity of 0.1, but are not much lower than the cloud threshold of 0.35, these cases are inferred as rather cloudy with cloud amounts of 0.554 and 0.382, respectively, for the two cases.

For the cases of 8, 17, and 19 September, the mean brightness temperature of the Huayin region is low (<270 K) but the mean reflectivity is high (>0.37). These cases can be considered very cloudy. The brightness temperature and reflectivity for the individual pixels are shown in Fig. 6. The pixels for the other two cases (4 and 9 September) are shown in Fig. 7. They are not as cloudy as those shown in Fig. 6. It is noted that the cloud parameters are inferred assuming no aerosols in the atmosphere. Therefore, the inferred cloud parameters represent not only the actual clouds but also the aerosols.

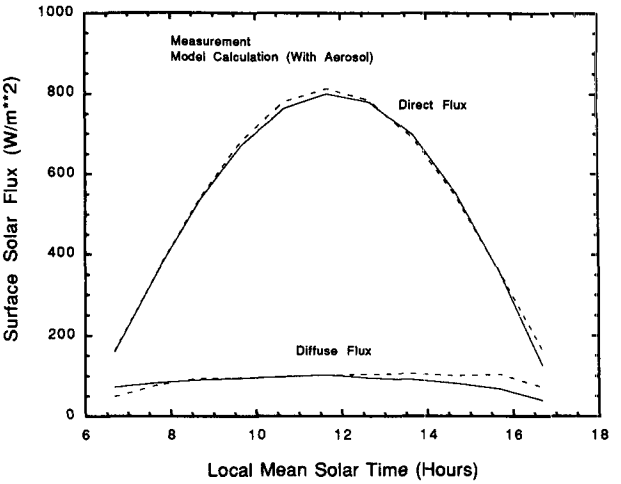

FIG. 5. The diurnal variation of the direct and diffuse downward solar fluxes at the surface for 5 September 1988. The solid curves are surface measurements, and the dashed curves are model calculations.

Using the inferred cloud parameters, the radiosonde temperature and humidity profiles, and the U.S. Standard Atmosphere ozone profile, surface solar and thermal IR fluxes are computed for the eight cases. Because there are discrepancies between the time of flux measurements and the time of radiosonde measurements, the temperature and humidity profiles are interpolated according to the procedures given in the previous section. Furthermore, there is discrepancy between the time of satellite passes and the time of surface measurements, as can be seen in Tables 1 and 2. The solar zenith angle and the temperature and humidity profiles used for the flux calculations correspond with the time of surface radiation measurements. Cloud parameters used correspond, however, with the time of satellite passes. If clouds change rapidly during these times, it might induce a large error in the flux calculations. In order to reduce the degree of complexity in comparing the computed and measured fluxes, we have used the broadband surface reflectivity deduced from surface flux measurements. In practice, the surface reflectivity is not exactly known, and it will enhance the uncertainty in flux calculations.

The measured and the computed net downward surface solar fluxes for the eight cases are given in Table 2. The discrepancy is large for some cases. The mean error is 4.3 W m^{-2}, and the rms error is 17.4 W m^{-2}. The discrepancy is believed to be caused primarily by the time difference between the surface and satellite measurements and by the uncertainty in cloud retrieval.

For the three cases that are believed to be cloud-free, the net downward surface solar flux is overestimated in the 5 and 10 September cases but underestimated

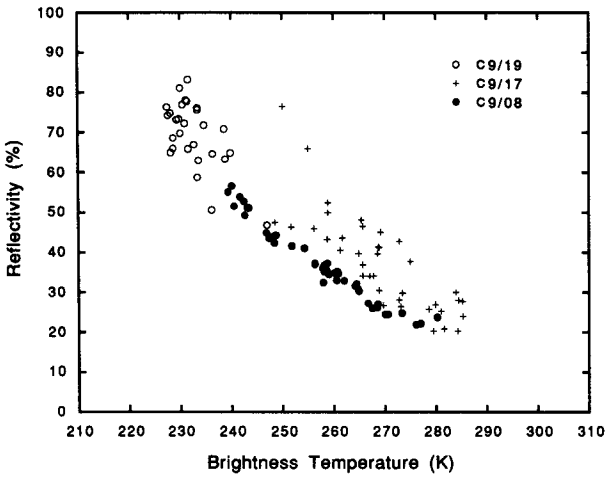

FIG. 6. Same as Fig. 2 except for the three large-cloudiness cases.

in the 6 September case. Compared to the 6 September case, the mean reflectivity (α_1 in Table 1) of the Huayin region for the 5 September case is larger (0.241 vs 0.202), but the calculated downward surface solar flux is also larger (399.0 vs 352.8 W m^{-2}). This discrepancy is likely to be caused by the misinterpretation of aerosols as clouds. As can be seen in Fig. 2, all the pixel reflectivities are below the cloud threshold of 0.35, and the mean cloud reflectivity is set to 0.35. Because of a larger satellite zenith angle for the 5 September case than the 6 September case (36.54° vs 22.42°), the inferred cloud optical thickness for the former case is only half of that for the latter case (2.3 vs 5.5). This discrepancy is erroneous and is a result of using the scattering phase function of cloud droplets. Furthermore, the single-scattering albedos are different for aerosols and for clouds. Errors are induced in the surface radiation calculations when a single-scattering albedo representing cloud droplets is used in dusty atmospheres.

For the three cases involving large cloudiness, 8, 17, and 19 September, the computed surface solar fluxes are in reasonable agreement with the measured fluxes, except for the 19 September case. There are several reasons for the large surface flux error. (a) As can be seen in Fig. 6, all pixels for the 19 September case have low brightness temperature (<248 K) and high reflectivity (>47%). The estimated cloud amount is 1.0 and optical thickness is 11. Because the cloud reflectivity is not sensitive to the optical thickness for thick clouds, the error in the cloud optical thickness might be large for large cloud reflectivity. This could induce large errors in the surface solar flux calculations due to the uncertainty in the single-scattering albedo. (b) As judged from the low brightness temperature, the clouds are believed to be high and are likely to contain ice particles. The cloud asymmetry factor and single-scattering albedo used in the flux calculations are typical for water clouds but not appropriate for ice clouds. (c) The spatial variability in the cloud properties is large, as is shown by the large range of reflectivity. Clouds at the measurement site may not be representative for the larger 2.5° × 2.5° latitude–longitude region.

The measured and calculated downward IR fluxes at the surface are also given in Table 2. The rms error is 22.1 W m^{-2}, but the mean error is only −4.66 W m^{-2}. This error is believed to be caused primarily by the uncertainty in temperature and humidity interpolations. The upward surface IR fluxes are dependent upon the ground temperature and emissivity. The daytime ground temperature in the arid Huayin region could change by >10°C h^{-1} at noontime. Because we do not have reliable information on the ground temperature and emissivity, the upward IR fluxes are not computed.

The foregoing results correspond to the use of a cloud threshold of 0.35 and a clear-column reflectivity of 0.10. We also have computed the surface fluxes using a cloud threshold of 0.25 and/or a clear-column reflectivity of 0.15. It has been found that the surface solar and IR fluxes computed with the use of a cloud threshold of 0.25 differ only marginally (<10 W m^{-2}) with those computed with a cloud threshold of 0.35. The use of different clear-column reflectivities of 0.1 and 0.15 causes a larger effect. Large discrepancies ($\approx$20 W m^{-2}) are found in relatively clear cases when the cloudy-column reflectivity is low. It indicates that the computed cloud amount is sensitive to the clear-column reflectivity, as can be seen in (1). The assumed cloud thickness has a small effect on the IR fluxes. The surface IR fluxes increases by less than 8 W m^{-2} when the thickness of a cloud layer increases from 50 to 100 mb.

7. Concluding remarks

We have investigated the uncertainty in estimating the surface radiation by coupling theoretical radiative transfer calculations with satellite cloud retrievals. In the surface radiation calculations, the temperature and humidity measured in the Huayin region and the cloud parameters inferred from the radiances measured by channels 1 and 4 of the *NOAA-9* AVHRR are used. Comparisons with the surface measurements of solar fluxes show that large discrepancy occurs in some cases. The discrepancy is attributable primarily to the lack of aerosol information, the uncertainty in the cloud parameters, the uncertainty in the flux measurements, and the time difference between the surface and satellite measurements.

For the clear cases, as identified from satellite reflectivity and brightness-temperature measurements, the computed surface fluxes assuming no aerosols are significantly larger (>100 W m^{-2}) than the surface

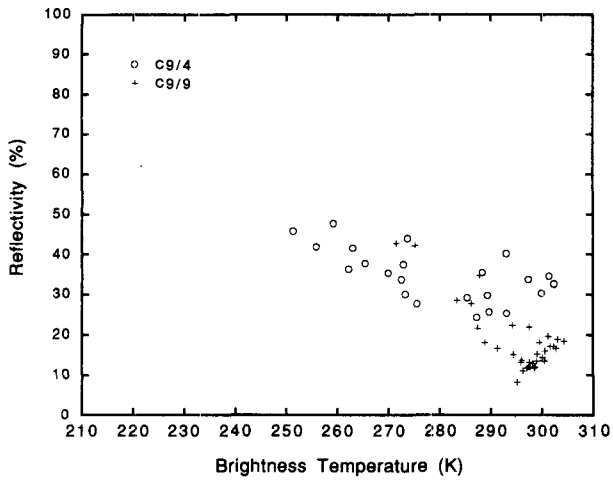

FIG. 7. Same as Fig. 2 except for the two medium-cloudiness cases.

measurements in the late afternoon. Because the uncertainty in the atmospheric humidity and ozone contents is not expected to induce such a large difference, it is concluded that the the exclusion of aerosols in the flux calculation is the main cause for the large difference.

In the Huayin area, there is a strong diurnal surface temperature variation. The temperature is higher by tens of degrees Celsius in the afternoon than in the early morning. Therefore, the atmosphere is expected to be much less stable in the afternoon. This phenomenon, plus the fact that the ground has little vegetation coverage, might lead to a dusty atmosphere in the afternoon. This expectation is consistent with the smaller solar flux measured in the afternoon than in the morning in cloud-free situations. Unfortunately, we cannot substantiate this expectation because of the lack of aerosol information. The result, however, reemphasizes the importance of providing aerosol information, either from surface or satellite measurement, for atmospheric energy budget and remote sensing studies.

One of the sample cases can be identified as totally cloudy because of a very low brightness temperature and high reflectivity. The computed surface solar flux is significantly smaller than the surface measurements. The error is believed to be caused by uncertainties in the inferred cloud optical thickness and prescribed single-scattering albedo. The cloud optical thickness is related to the cloud reflectivity in a highly nonlinear fashion. For thick clouds, reflectivity is not very sensitive to the optical thickness, and the uncertainty in the inferred cloud optical thickness could be large. Furthermore, the single-scattering albedo is prescribed based on the aircraft measurements of stratocumulus clouds. Thus, it may not be representative of the clouds in the Huayin region. For this cloudy case, the inferred optical thickness is relatively large, and the uncertainty in the prescribed single-scattering albedo could induce a large error in the surface solar flux calculations.

Because of the inadequate information on the cloud and aerosol parameters, the uncertainty in the computed surface solar flux using a radiative transfer routine is expected to be large. However, the uncertainty in the surface solar flux estimation can be reduced by imposing certain constraints on the radiative transfer calculations. Instead of computing directly the solar radiation absorbed at the surface, the partitions of the solar radiation absorbed in the atmosphere and at the surface can be more accurately computed from a radiation routine. The surface radiation can then be derived from the satellite-measured fluxes at the top of the atmosphere, such as the Earth Radiation Budget Experiment (ERBE) and (Barkstrom et al. 1990), and from the computed partitions of the solar radiation absorbed in the atmosphere and at the surface.

For the calculation of surface IR fluxes, the temperature and humidity data available to us are far from adequate, especially in this arid region where temperature changes rapidly from hour to hour. Nevertheless, the computed surface IR fluxes compare favorably with the measured fluxes. More information on temperature and humidity, as well as dust particles, either from surface measurements or from satellite retrievals, is required to enhance the accuracy of IR flux calculations.

Acknowledgments. The work conducted at Goddard Space Flight Center and at the University of Utah (Grant NAG5-1050) was supported by the NASA Radiation Processes Program managed by Dr. Timothy Suttles.

REFERENCES

Barkstrom, B. R., E. F. Harrison, and R. B. Lee, III, 1990: Earth Radiation Budget Experiment: Preliminary seasonal results. *Eos*, **71**, 297–305.

Chou, M.-D., 1986: Atmospheric solar heating rate in the water vapor bands. *J. Climate Appl. Meteor.*, **25**, 1532–1542.

——, 1989: On the estimation of surface radiation using satellite data. *Theor. Appl. Climatol.*, **40**, 25–36.

——, 1990: Parameterizations for the absorption of solar radiation by O_2 and CO_2 with application to climate studies. *J. Climate*, **3**, 209–217.

——, 1991: The derivation of cloud parameters from satellite-measured radiances for use in surface radiation calculations. *J. Atmos. Sci.*, **48**, 1549–1559.

——, 1992: A solar radiation model for climate studies. *J. Atmos. Sci.*, **49**, 762–772.

——, D. P. Kratz, and W. Ridgway, 1991: Infrared radiation parameterizations in numerical climate models. *J. Climate.*, **4**, 424–437.

D'Almeida, G. A., 1987: On the variability of desert aerosol radiative characteristics. *J. Geophys. Res.*, **92**, 3017–3026.

Darnell, W. L., W. Staylor, S. K. Gupta, and F. M. Denn, 1988: Estimation of surface insolation using sun-synchronous satellite data. *J. Climate*, **1**, 820–835.

Gautier, C., G. Diak, and S. Masse, 1984: An investigation of the effects of spatially averaging satellite brightness measurements

on the calculation of insolation. *J. Climate Appl. Meteor.*, **23,** 1380–1386.

Gupta, S. K., 1989: A parameterization for longwave surface radiation from sun-synchronous satellite data. *J. Climate,* **2,** 305–320.

Holben, B. N., Y. J. Kaufman, and J. D. Kendall, 1990: *NOAA-11* AVHRR visible and near-IR inflight calibration. *Int. J. Remote Sens.*, **11,** 1511–1519.

Justus, C. G., M. V. Paris, and J. D. Tarpley, 1986: Satellite-measured insolation in the United States, Mexico, and South America. *Remote Sens. Environ.*, **20,** 57–83.

Kaufman, Y. J., and B. N. Holben, 1992: Calibration of the AVHRR visible and near-IR bands by atmospheric scattering, ocean glint and desert reflection. *Int. J. Remote Sens.*, in press.

King, M. D., L. F. Radke, and P. V. Hobbs, 1990: Determination of the spectral absorption of solar radiation by marine stratocumulus clouds from airborne measurements within clouds. *J. Atmos. Sci.*, **47,** 894–907.

Lacis, A. A., and J. E. Hansen, 1974: A parameterization for the absorption of solar radiation in the earth's atmosphere. *J. Atmos. Sci.*, **31,** 118–133.

Liou, K.-N., Q. Fu, and T. P. Ackerman, 1988: A simple formulation of the delta-four-stream approximation for radiative transfer parameterizations. *J. Atmos. Sci.*, **45,** 1940–1947.

Nakajima, T., M. D. King, J. D. Spinhirne, and L. F. Radke, 1990: Determination of the optical thickness and effective particle radius of clouds from reflected solar radiation measurements. Part II: Marine stratocumulus observations. *J. Atmos. Sci.*, **47,** 1878–1893.

Pinker, R. T., and I. Laszlo, 1990: Improved prospects for estimating insolation for calculating regional evapotranspiration from remotely sensed data. *Agric. For. Meteor.*, **52,** 227–251.

Schmetz, J., 1989: Towards a surface radiation climatology: Retrieval of downward irradiances from satellites. *Atmos. Res.*, **23,** 287–321.

Shettle, E. P., and R. W. Fenn, 1979: Models for the aerosols of the lower atmosphere and the effects of humidity variations on their optical properties. AFGL-TR-0214, 94 pp.

Tsay, S.-C., G. L. Stephens, and T. J. Greenwald, 1991: An investigation of aerosol microstructure on visual air quality. *Atmos. Environ.*, **25A,** 1039–1053.